



OPEN Experimental investigation on mechanical properties of iron metal matrix reinforced with MAX phase V₂AlC-GO

Engidayehu Mekonnen Alemu¹, Jana Petru²✉, Muhammad Nasir Bashir^{2,5}, Abdulrahman Aljabri^{3,4}, Joon Sang Lee⁵, Irfan Anjum Badruddin⁶, Bilal Akbar Chuddher⁷, M. A. Fazal⁸, Sami Ghazali⁸, Abdulmalik Alkotami⁸ & Gulam Mohammed Sayeed Ahmed^{1,9}✉

The development of high-quality composites has become increasingly crucial due to rapid modernization and technological advancements, particularly as traditional iron-based materials face significant limitations such as high density, low strength-to-weight ratios, and susceptibility to corrosion and wear. This research focuses on fabricating a metal matrix composite (MMC) from a pure iron matrix reinforced with vanadium aluminum carbide (V₂AlC) and graphene oxide (GO) using the powder metallurgy method, followed by testing its mechanical properties. The microstructural features of the samples were examined using Optical Microscopy and X-ray Diffraction, while the Archimedes method assessed density and porosity. Mechanical analyses, including hardness, compressive strength, and corrosion resistance, were conducted in accordance with ASTM standards, with corrosion resistance evaluated using an electrochemical analyzer. Initially, nine samples containing 5 wt.% V₂AlC and 4 wt.% GO were fabricated by varying key powder metallurgy parameters, which were optimized using Taguchi-based grey relational analysis. Following this, four additional samples with varying V₂AlC percentages (5%, 8%, 10%, and 15%) were created based on the optimal parameters. The results indicated significant improvements in the physical, mechanical, and corrosion resistance properties of the optimally fabricated composites, characterized by uniformly dispersed reinforcements and distinct phases. This enhanced iron MMC is proposed for high-performance applications in the automotive, aerospace, and marine industries, thereby addressing the limitations of traditional materials and contributing to advanced material solutions.

Keywords Iron hybrid metal matrix composite, Vanadium aluminum carbide, GRA, Mechanical properties, Powder metallurgy

The production and innovation of advanced materials that meet the demands of new applications represent a critical area of research in the manufacturing industry. Metal matrix composites (MMCs) are a notable type of composite material created by combining two or more components, resulting in superior properties compared to the parent materials. Typically reinforcing elements in MMCs include ceramic whiskers, continuous or discontinuous fibers, and particles^{1–4}. These composites are increasingly recognized for their promising capabilities and are utilized across various industrial sectors, including automotive, aerospace, defense, marine, and electronics. The incorporation of hard particulates enhances operational performance and wear resistance^{5–8}.

¹Department of Mechanical Engineering, Program of Manufacturing Engineering, Adama Science & Technology University, 1888 Adama City, Ethiopia. ²Department of Machining, Assembly and Engineering Metrology, Faculty of Mechanical Engineering, VSB Technical University of Ostrava, Ostrava, Czech Republic. ³Department of Mechanical Engineering, Islamic University of Madinah, 42351 Medina, Saudi Arabia. ⁴Sustainability Research Center, Islamic University of Madinah, 42351 Madinah, Saudi Arabia. ⁵Multi-Scale Fluid Dynamics Lab, Department of Mechanical Engineering, Yonsei University, Seoul 120-749, Republic of Korea. ⁶Mechanical Engineering Department, College of Engineering, King Khalid University, 61421 Abha, Saudi Arabia. ⁷Industrial Engineering Department, College of Engineering, King Khalid University, 61421 Abha, Saudi Arabia. ⁸Department of Mechanical and Materials Engineering, University of Jeddah, Jeddah, Saudi Arabia. ⁹Department of Mechanical Engineering, Centre of Excellence (COE), Advanced Manufacturing Engineering, Adama Science & Technology University, 1888 Adama, Ethiopia. ✉email: jana.petru@vsb.cz; gmsayeed.ahmed@astu.edu.et; drgmsa786@gmail.com

In this research work, commercially available iron powder with a purity of 99.8% is selected as the matrix for fabricating a hybrid composite. Fine powder of vanadium aluminum carbide (V_2AlC) is utilized as the primary reinforcement material, while graphene oxide (GO) powder is added to control friction during the mixing and compaction processes, as a dry lubricant^{9–12}. Iron-based reinforced MMCs are in demand due to their improved strength, high modulus and increased wear resistance compared to conventional iron alloys^{9,13–15}. V_2AlC is a ternary nano-laminated hexagonal compound that belongs to the family of MAX phases, characterized by the general formula M_n+1AX_n , where M denotes the transition metal, A represents a metal, and X signifies carbon or nitrogen as presented^{16–19} in Fig. 1. These materials exhibit exceptional properties associated with both ceramics and metals, including a low friction coefficient, good electrical and thermal conductivity, excellent machinability, and superior resistance to oxidation and corrosion. V_2AlC stands out due to its lower density (4.81 g/cm^3), high thermal conductivity ($48\text{ W/m}\cdot\text{K}$) and outstanding bulk modulus (215 GPa). These remarkable physical properties, V_2AlC shows great promise for applications as tough wear resistant coatings and polycrystalline thin films across various substrates. Furthermore, research interest in V_2AlC ceramics is highlighted by the potential to obtain a two-dimensional carbide, V_2C M-Xene, through the selective etching of aluminum layers from V_2AlC ^{20–24}.

The primary goal of mixing of these ingredients is to achieve a uniform distribution of reinforcement particles within the matrix metal powder. Factors such as compaction pressure, compaction speed, dwell time significantly affect the density, dimensional accuracy and mechanical properties of the green compact^{25–29}. Lubricants like graphite or molybdenum sulfide are often employed between the die wall and the powder to facilitate die compression. The sintering process involves a heat treatment applied to the green compact at high temperatures, below the melting point of the primary constituent, in a controlled atmosphere. This process enhances the bonding between particles and increases the strength of the powder metal compact, resulting in the desired properties of the final product⁸. Additionally, post-sintering processes such as heat treatment, machining, surface finishing, and coating can further refine the properties and surface characteristics of the sintered parts^{30,31}. An attempt has been made in this work to produce an iron-based metal matrix composite (MMC) reinforced with vanadium aluminum carbide (V_2AlC), incorporating a small amount of graphene oxide (GO) powder to control friction during the mixing and compaction processes, as GO is widely recognized as an effective dry lubricant for automotive and industrial applications. The fabrication of the iron-based MMC was carried out using powder metallurgy techniques, with the synthesis conducted under varying powder metallurgy (PM) process parameters and different weight percentages of reinforcing particulates. The study focuses on synthesizing and analyzing the effects of key PM parameters—such as milling time, compaction pressure, sintering temperature, and weight percentage of reinforcement—on the properties of the iron matrix with V_2AlC MAX phase. Additionally, the research investigates mechanical properties, including hardness and compressive strength, as well as physical properties like density. To determine the optimal values of these parameters, Multi-Response Analysis (MRA) and Genetic Algorithms (GA) will be employed. Various experiments and tests, including hardness and compression strength evaluations, will be conducted along with sample characterization using X-ray Diffraction (XRD) and Scanning Electron Microscopy (SEM). Another attempt has been made in this work to enhance the mechanical and metallurgical performance of the generated composites by integrating MAX phase materials like V_2AlC and utilizing GO as a lubricant, thereby addressing the need for materials with higher specific strength, hardness, and dimensional stability at elevated temperatures. MAX phase materials, represented by the general formula $M_{n+1}AX_n$ (where $n = 1–3$), consist of layered carbide and nitride compounds that have potential applications in structural and functional fields. Their unique properties make them ideal candidates for strengthening metal matrix composites, with significant technological applications identified in areas such as nuclear power, high-speed rail, gas igniters, heat exchangers, high-thrust rocket nozzles, electric brushes, metal refining electrodes, and high-temperature seals. In this work they found that addition of boron carbide particles to Al7075 alloy to enhance the composite's hardness and tensile strength, which are required for critical automotive parts. The distribution of the B4C particles within the aluminium matrix leads to enhanced strength, reduced porosity, better strength-to-weight ratio. In other studies, it was shown that by integrating zirconium silicate into Al6063, the alloy shows significantly enhanced Impact, compression strength and impact strength with optimal results achieved at around 6% zirconium silicate content. The inclusion of B4C particles in Al6066 enhanced the composite's resistance in dry sliding wear mechanism with higher B4C content correlating to reduced wear volume and improved Hardness due to the uniform dispersion of hard B4C particulates within

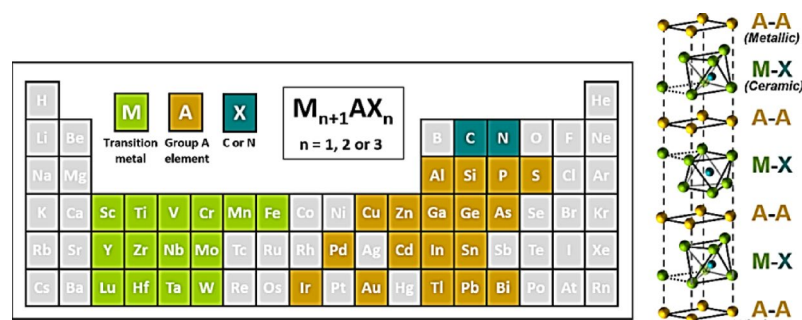


Fig. 1. Elements of the periodic table found in MAX phases and unit cell for $n = 1$,¹².

Element	%	Element	%
Carbon	0.004	Silicon	0.001
Manganese	0.04	Phosphorous	0.004
Sulphur	0.007	Aluminum	0.001
Arsenic	0.002	Boron	0.001
Nitrogen	0.006	Niobium	0.001
Tin	0.001	Titanium	0.001
Vanadium	0.001	Lead	0.002
Bismuth	0.001	Calcium	0.0002
Tellurium	0.001	Hydrogen	1.1 ppm

Table 1. Composition of commercial pure iron.

Mechanical properties	Metric	English
Strength at break	540 MPa	78,300 psi
Yield strength	50 MPa	7250 psi
Poisson's ratio	0.291	0.291
Modulus of elasticity	200 GPa	29,000 ksi
Shear modulus	77.5 GPa	11,200 ksi
Hardness, Vickers	150	150
Density	7.87 g/cm ³	0.284 lb/in ³
Melting point	1536 °C	2797°F
Boiling point	2861 °C	5182°F

Table 2. Mechanical and physical properties of pure iron.

the matrix^{32–34}. In this research work they found that PETG's tribological properties can be enhanced with reinforcement of carbon fibers or graphene, but in FDM PETG tends to wear faster than polymers due to its lower hardness. By incorporating CeO₂ and GNPs leads to enhanced hardness, notably composites containing 3 wt.% CeO₂ and GNPs achieved considerable increases in hardness and overall mechanical strength. Recycling aluminium combined with using waste materials as reinforcements to produce lightweight and high-strength composites with improved mechanical and physical properties. This article reviews different recycling techniques, including mechanical grinding and powder metallurgy, relevant for converting aluminium waste into particulate reinforcements in matrix^{35–37}. In this investigation, MXenes inherit many advantageous properties from their parent MAX phases, including electrical conductivity and mechanical stability due to their 2D layered structure to enhanced surface reactivity and greater ion accessibility in hybridization of MXenes with carbon materials such as graphene in metal oxides to enhances their electrochemical performance and stability³⁸. In this work the presence of TiC crystals enhanced the coefficient of friction (COF) and wear resistance under load bearing test conditions. In Tribological tests reveals that the coatings perform better in liquid compared to air³⁹. In this investigation hot press sintering, chemical vapor deposition and molten salt synthesis, which provide variations in temperature and pressure to optimize phase purity and microstructure. They have also revealed low temperature molten salt methods reduces synthesis temperature by enhancing diffusion and reaction rates leading to nanosized MAX phases to attain improved purity⁹. In another work the authors explored the effect of feed rate and metal cutting speed on cutting forces during machining of epoxy-based bio-composites reinforced with almond shell and coconut fiber particles. The biocomposites' machining behavior depends strongly on the reinforcement content, with higher particle loads leading to increased cutting forces due to increased material hardness¹⁰.

Materials and methods

To ensure the appropriate selection of matrix and reinforcement materials for the intended research, it is crucial to possess a comprehensive understanding of the properties and applications of both the matrix and reinforcing materials. The Cast iron composition as given in Table 1, with carbon, nickel, chromium, and other elements.

Iron powder was chosen since it is stronger and suitable for a number of uses in the construction and automotive industries in order to function better in metal matrices by creating heat. Table 2 shows the pure iron powder that was purchased from Parshwamani metal manufacturers India, having an average particle size of (150 µm), density 7.874 g/cm³ at 25 °C and 99.99% purity used as matrix.

Vanadium aluminum carbide powder

Physical properties of V₂AlC materials given in Table 3, possess spectacular performances associated with either ceramics or metals, such as excellent machinability, good electrical and thermal conductivity, low friction coefficient as well as superior resistance to oxidation and corrosion of these MAX phases.

Properties	Metric
Molecular weight	140.87
Melting point	2000 °C
Density	4.85 g/cm ³

Table 3. Physical properties of V₂AlC.

No	Fe %	V ₂ AlC %	GO %	MT (hrs.)	CP (MPa)	ST (°C)
S _{1.1}	91	5	4	1	70	1100
S _{1.2}	91	5	4	1:30	60	1100
S _{1.3}	91	5	4	2	50	1100
S _{1.4}	91	5	4	1	50	900
S _{1.5}	91	5	4	1:30	70	900
S _{1.6}	91	5	4	2	60	900
S _{1.7}	91	5	4	1	60	1000
S _{1.8}	91	5	4	1:30	50	1000
S _{1.9}	91	5	4	2	70	1000

Table 4. Reinforced IMMC manufactured through powder metallurgy (sample 1).

Sample's	Materials (in weight %)			Process parameters		
	Fe (%)	V ₂ AlC (%)	GO (%)	MT	ST	CP
S ₂	91	5	4			
S ₃	88	8	4			
S ₄	86	10	4			
S ₅	81	15	4			

Table 5. Reinforced IMMC manufactured through powder metallurgy (S₂, S₃, S₄ & S₅).

Graphene oxide

Graphene oxide (GO), also referred to as graphite/graphitic oxide, is produced by treating graphite with oxidizers, and results in a compound of carbon, oxygen, and hydrogen in variable ratios.

Design of experiment for IMMC fabrication

In this work, a powder metallurgical process was used to prepare iron matrix composite samples reinforced with V₂AlC/GO. Nine samples were synthesized and chosen for constant weight reinforcement ratio with different powder metallurgy process parameters, developed by L₉ orthogonal array and the rest three samples had been manufactured with optimal process parameters for varied weight ratio as shown in Table 4. The powder metallurgy-based input process parameters (milling time, Compaction Pressure, Sintering Temperature and weight fraction of reinforcement). Whereas, for the rest four samples mentioned in Table 5, were manufactured with optimal process parameters based on previously manufactured and tested samples with better properties.

Powder mixing

In order to achieve the desired performance of the selected powders in the manufacturing of composites, mixing refers to the homogeneous blending of different types of powders, and it is essential to distribute them evenly throughout the matrix. This has been accomplished through the use of high energy ball milling machines. Zirconia balls shown in Fig. 2, are used to ball mill metal alloy powders in a high velocity chamber.

In this study 5% of V₂AlC and 4% GO powder were mixed with 91% of pure iron in sample one for fabricated nine samples (three trial samples for each) with different powder metallurgy process parameters for first round and then 5%, 8%, 10% and 15% of V₂AlC were mixed with 88%, 86% & 81% of pure iron respectively at constant 4% of GO for the rest four samples at optimal PM process parameters. A high energy planetary ball mill was used to mix the powder by using zirconia balls. The Milling Parameters used in the ball milling process are Milling speed: 200 rpm, Milling time: 1, 2 and 3 h, Ball diameter: 10 mm, Ball to powder weight ratio: 10:1, Temperature of milling (at room temperature).

Powder compaction

Powder compaction is the process of compressing the Fe-V₂AlC-GO mixed powder in a mold using a hydraulic mounting press. The combined powder was accurately measured with a weighted balance. The powder mixture

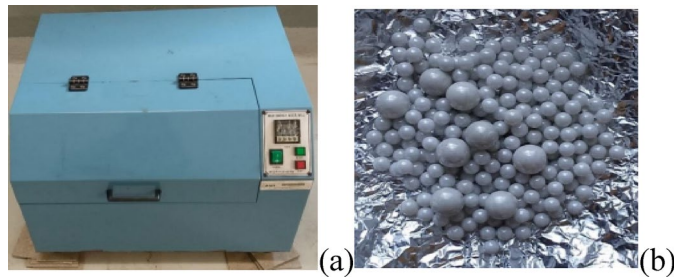


Fig. 2. (a) High energy mixer/mill machine (b) zirconium balls.

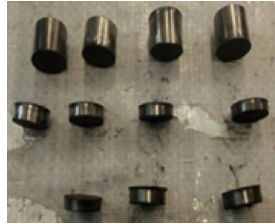


Fig. 3. Compacted specimen (Green Part).

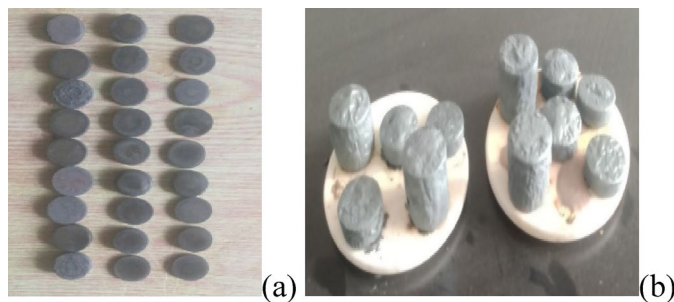


Fig. 4. (a) Green compact (b) sintered samples.

was pressed into a cylindrical shape ($d = 12$ mm, $h = 20$ mm) as shown in Fig. 3, using a carbon steel die using a hydraulic press with a load of 120 KN. Cold pressing was performed at a pressure of 50, 60 & 70 MPa (Olani et al., 2023) and a holding time of 10 min. The density of compacted powders is directly proportional to the pressure applied.

Sintering

The green compressed sample's does not have sufficient strength and the particles are loosely bound together and may crash easily at low loads. After deformation, particle formation and growth, and cooling, the powders combine to form solid pieces as shown in Fig. 4a and b. During sintering, bonding occurs between agglomerated powder particles. After the manufacturing of composite materials those fabricated through different powder metallurgy process parameters (milling time, compaction pressure and sintering temperature) physical and mechanical properties were tested.

Density of composite materials

In this stage density were tested for developed nine samples (three trial for each) based on powder metallurgy process parameters. Density is a physical property of a material that describes its mass per unit volume. It is an important property of materials, particularly in engineering applications where weight and strength are critical factors. The composition and structure of the MMCs, as well as the manufacturing method used to produce them, can affect density. In this research, the density of the specimens was measured using the Archimedes method to identify the effects of powder metallurgy process parameters and reinforcements. As per ASTM B962-23, the surface roughness of the specimens was removed using 120-grit sanding, and surface pores were sealed by oil impregnation. The relation for calculating the density of the specimen by Archimedes method is as follows $\rho_{\text{sample}} = \frac{W_{\text{Air}} \times \rho_{\text{Fluid}}}{W_{\text{Air}} - W_{\text{Fluid}}}$, Where: ρ_{sample} = Sample density, W_{Air} = Sample weight in the atmospheric air,

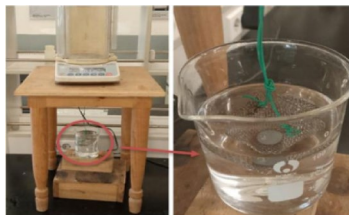


Fig. 5. Archimedes method of density measurement in distilled water.

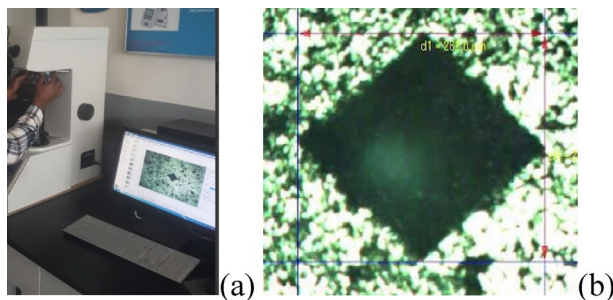


Fig. 6. Vickers hardness test and measurement.

W_{Fluid} = Sample weight in the fluid, ρ_{Fluid} = Fluid/Water density (0.9982 g/mL at 20 °C).

Porosity of composite materials

Porosity is the existence of space or pores in the structure of composite materials. It represents the fraction of overall volume of the composite that is occupied by these void spaces. The porosity is denoted by the symbol ϕ , and its value ranges between 0 and 100% when it is expressed as a percentage or between 0 and 1 when it is expressed as a fraction. In this study Archimedes' method shown in Fig. 5, was employed based on the principle of buoyancy and widely used for porosity determination in MMCs.

Hardness test

It is a very important test in engineering applications that shows a material's ability to withstand wear, friction, and erosion by external factors. In this work, Vickers hardness test method was used, by measuring the indentation Fig. 6b, on specimen's surface using a diamond indenter in the shape of a square-based 136° pyramid with a specific load to the specimen's surface by using hardness testing machine (HVS-50) shown in Fig. 6a.

By apply a uniform load without impact and push the indenter into the specimen. The load used for hardness test was 10kgf with 5 s holding time. This test was conducted as per ASTM-B933-16 for all specimens. The Vickers hardness number is calculated using the formula $HV = \frac{\text{Constant} \times \text{Test force}}{\text{Surface area of indentation}} = \frac{1.854F}{d^2}$, where HV = Vickers Hardness number, F = Applied load in kgf, d = Length of the diagonals of the indentation in mm.

Compression strength test

Compressive strength of a material is the ability of the material to withstand compressive loading without failure. In this study the compression test was conducted on optimized samples under uniaxial compressive loading on a UTM with a 50 KN capacity at room temperature at ASTU, Mechanical lab. The ASTM E9 standard was used for this work includes specimens and steps for axial compression testing at room temperature and considerations for specimen geometry. The compressive strength of the samples shown in Fig. 7, after sintering was measured by a compression testing machine universal testing machine with a strain rate of 10 s⁻¹ at room temperature.

Data analysis and optimization method

The process parameters (such as milling time, compacting pressure and sintering temperature) were analyzed through Taguchi-based GRA optimization technique, based on the experimental results obtained from physical tests and mechanical tests. GRA based Taguchi method is appropriate for data analysis to provide an optimum sample during the analysis of multiple responses using the response graph method.

Step 1: Change the replicated response data into the S/N (η) ratio (X_i) using the following formulas For the smaller better, $\eta = -10 \log \left[\frac{1}{n} \sum_{i=1}^n X_{ij}^2 \right]$, For the larger better, $\eta = -10 \log \left[\frac{1}{n} \sum_{i=1}^n \frac{1}{X_{ij}^2} \right]$, Where η = Signal to noise ratio, X_{ij} = experimental value per trial, n = number of replication, and i = number of trial.

Step 2: Normalize the data in order to eliminate the influence of different measurement units and to ensure that all the data sets are transformed into comparable ranges. After this process, the data values obtained range between 0 and 1. Since the objective of this study is to minimize the density and increase strength and hardness, the smaller the better and larger the better for hardness and density were taken for analyzing the

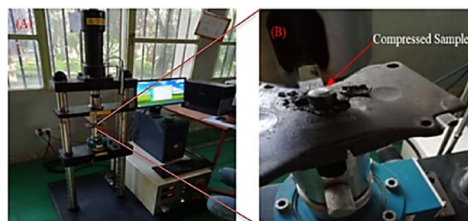


Fig. 7. UTM (compression test) with compressed sample.

quality respectively, the equation of larger the better were used as $Y_{ij} = \frac{X_{ij} - \min(X_{ij})}{\max(X_{ij}) - \min(X_{ij})}$ and the formula of the smaller the better for porosity normalization method is, $Y_{ij} = \frac{\max(X_{ij}) - X_{ij}}{\max(X_{ij}) - \min(X_{ij})}$, Where: Y_{ij} = normalized value for i th trial for j th response, X_{ij} = S/N ratio value for i th trial for j th response, i = trial number ($i = 1, 2, \dots, n$) and j = response number ($j = 1, 2, \dots, m$).

Step 3: Compute the coefficient of grey relational for the normalized values (Kuo et al., 2008; P. K. Sahu & Pal, 2015). $\delta_{ij} = \frac{\Delta_{\min} + \Upsilon \Delta_{\max}}{\Delta_{ij} + \Upsilon \Delta_{\max}}$, Where: δ_{ij} = grey relational coefficient for the i th trial and j th, Δ = deviation sequence of reference value i th and j th normalized value of the responses, Δ_{\max} & Δ_{\min} denotes the maximum and minimum values of “ Δ ” respectively, Υ = maximum value of normalized S/N ratio distinguishing coefficient which is defined in the range $0 \leq \Upsilon \leq 1$.

Step 4: Calculate the grey relational grade (β_i). At the last, the grey relational grades were calculated using Eq. (1) for selecting optimal levels for the process parameter. Optimal level for factors as well as influential process parameter was analyzed further using the response graph method. $\beta_i = \frac{1}{m} \sum \delta_{ij}$, Where: m = number of responses. In this study two experiment were investigated, the first experiment was examined the samples fabricated with different powder metallurgy process parameters, at fixed reinforcement (5% of V_2AlC with 4% of GO as lubricant) for all nine samples and next experiment was studied for samples fabricated based on optimal process parameters (5% of V_2AlC) and the rest three samples fabricated and examined with varying reinforcement (8%, 10% & 15% of V_2AlC with 4% GO) to investigate the effect of reinforcement at optimal level.

Specimen preparation for microstructural characterization

The sintered Fe- V_2AlC -GO composite samples were progressively finely grounded with a grinder for hardness testing and microstructural analysis. Polishing is the process of rendering the Fe- V_2AlC -GO composite samples scratch free using sandpapers of progressively increasing grit from 240, 800, 1200, and 2000. It was then exposed to grinding using sand papers from coarse to fine grades with orientation of 90° . Polishing is the process of rubbing the sample with a diamond suspension to create a smooth, shiny surface while gradually reducing the pressure and rotation speed of the sanding disc in the RB 204, Metpol II model polishing process. Polished samples were etched with the Nital solution of 4% nitric acid and alcohol mixed etchant for 30 s.

X-ray diffraction (XRD)

Phases analysis in sintered composite

XRD-7000 diffractometer Maxima model from Shimadzu Corporation has been employed for analyzing crystalline phases and elements of IMMC samples. Phase analysis of the sintered samples was performed by X-ray diffraction observation with Cu-K α radiation at 40 kV and 30 mA at 2θ value in between (80° - 100°) in 3° /min scan rate. Phase identification and quantitative phase analysis were performed by using origin pro 2022. The crystalline phase of the matrix and reinforcement's present in the sintered composite was analyzed.

Determination of crystalline size and lattice strain by XRD peak analysis

Gauss method of XRD peak profile analysis was employed to calculate the microstructural parameters namely crystalline size, mean squared lattice strain, root mean squared strain and dislocation density of Fe- V_2AlC -GO by using XRD data. By using the Scherer equation, we can quantitatively calculate the relationship between the diffraction peak and the crystal grain size. $D = \frac{K\lambda}{\beta \cos \theta}$, Where: D = Crystalline size, λ = XRD radiation of wavelength (μm), K = Shape factor can be 0.62–2.08. θ = Bragg's angle in degree. β is line of broadening at FWHM in radians or measurement of the full width at half maximum of the radian peak located at any 2θ . Dislocation density is a measure of the number of dislocations within a unit volume of the crystal. It was determined using XRD data with relate to crystalline size. $\delta = \frac{1}{D^2}$, Where: δ = Dislocation density in nm^{-2} , D = Crystallite size of the particles estimated from Scherer's equation. The local deviation of atoms in the crystal structure from their equilibrium position is known as lattice strain. The presence of non-uniform stress is typically caused by non-uniform stress causing peak broadening, mathematically calculated from XRD data, The Lattice Strain is given by $(\epsilon) = \frac{\beta}{4 \tan \theta}$.

Result and discussions

Density of composite materials

In this study density, porosity and hardness were analyzed in the first round based on the interrelation of powder metallurgy process parameters at fixed reinforcement 5% of V_2AlC and 4% of GO for nine samples and

Sample	Density (g/cm ³) 5% of V ₂ AlC			Average density
	1	2	3	
S ₁	6.4248	6.8555	6.8862	6.722
S ₂	5.5009	6.9711	7.0447	6.505
S ₃	6.2278	6.7709	6.8143	6.604
S ₄	6.6974	6.5995	6.6233	6.640
S ₅	7.0809	6.8095	6.7894	6.893
S ₆	6.7093	6.6661	6.7302	6.701
S ₇	7.1067	6.9168	7.0440	7.022
S ₈	6.0189	6.5905	6.6388	6.416
S ₉	6.8209	6.9122	6.4138	6.715

Table 6. Experimental density of Fe-V₂AlC-GO.

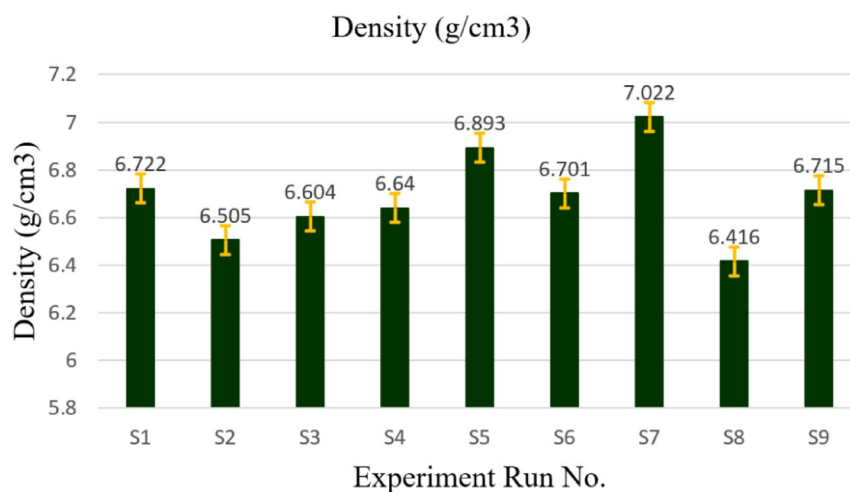


Fig. 8. Experimental density of Fe-V₂AlC-GO (5% V₂AlC).

optimization were performed, Table 6, shows the density of sintered samples for nine samples with three trials for different process parameters generated by L9 orthogonal array at fixed reinforcement. Figure 8, illustrates the experimental average density of developed samples by powder metallurgy process parameters (MT, CP and ST).

From the experimental test sample fabricated through A1B2C2 had higher density compared with others then is followed by A₂B₂C₃, this indicated that excessive sintering temperature can negatively impact by promoting excessive grain growth leading to increasing porosity and reduce overall density. High ST accelerate grain growth as grain become larger, they may not fill the spaces between them completely, leading to a decrease in density. Sample eight (A₂B₁C₂) had the lowest density compared with others this is due to the small compaction pressure because less force was applied to the powder particles, leading to less effective densification. The experimental test also investigated the effect of milling time on density of sintered samples (S₅, S₆ and S₉) had reduced density, sample fabricated through A₃B₃C₂ had higher MT, CP and moderate ST but the experimental result shows us the reduction on density due to excessive milling time.

Porosity of composite material

The porosity of fabricated composite samples was analyzed using the Archimedes technique. It was calculated from theoretical and experimental density as given in Table 7, Inadequate MT, CP, and ST all contribute to increased porosity. Particle clustering adversely affects the physical and mechanical properties and microstructure of PM parts.

Figure 9, shows the percentage of porosity within fabricated composite samples. In the figure observed that low percentage of porosity for S₇ and S₅ respectively and previously stated the density of composite material for S₇ and S₅ were higher, this indicate that porosity and density have an inverse relationship. The figure also illustrated that the highest percentage of porosity occurred for S₈ and S₂ respectively this shows the process parameters used to fabricate those samples were not suitable and leads to reduction of density.

Sample	Porosity (Φ)			Average porosity
	1	2	3	
S ₁	14.064	8.302	7.892	10.086
S ₂	26.421	6.756	5.771	12.982
S ₃	16.698	9.434	8.853	11.661
S ₄	10.417	11.727	11.408	11.184
S ₅	5.287	8.917	9.186	7.7965
S ₆	10.258	10.836	9.979	10.357
S ₇	4.942	7.482	5.781	6.068
S ₈	19.493	11.846	11.201	14.180
S ₉	8.765	7.544	14.210	10.173

Table 7. Experimental porosity of Fe-V2AlC-GO.

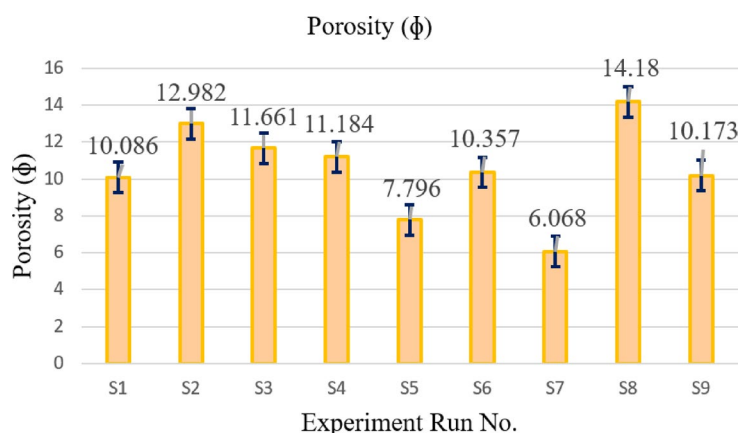


Fig. 9. Percentage of porosity with in Fe-V2AlC (5% V2AlC).

Sample	Vickers hardness (HV)			Average value
	1	2	3	
S ₁	327.2	316.1	304.1	315.8
S ₂	316.9	328.1	334.9	326.6
S ₃	325.2	323.3	312.3	320.2
S ₄	425.6	422.9	441	429.8
S ₅	342.2	317.7	342.7	334.2
S ₆	334	357.2	307.9	333.0
S ₇	360.7	312.3	374.3	349.1
S ₈	362.4	337.3	304.4	334.7
S ₉	408.1	389.5	440	412.5

Table 8. Experimental hardness values of Fe-V2AlC-GO composite.

Hardness of Composite Material

The hardness of the Fe-V2AlC-GO composite was tested using a Vickers hardness tester. Hardness tests were carried out on the composite specimen's surface in three different locations. The hardness values are presented in Table 8. The effect of process parameters on the hardness is clarified in Fig. 10.

From the experimental test the Average Hardness value shown in Fig. 10, the highest hardness observed for S₄ fabricated through A₁B₃C₃ and followed by S₉ (A₃B₃C₂) for both samples compression pressure was the same, for S₉ milling time increased to the highest level and sintering temperature was moderate but some reduction on hardness was occurred. On the other hand, S₇ (A₁B₂C₂) and S₉ had the same ST but decreasing on hardness compared with S₉, this is due to the reduction of compression pressure.

The lowest hardness occurred for S₁ (A₁B₁C₁) and followed by S₃ (A₃B₂C₃) because of low compaction pressure and sintering temperature, generally from the experiment samples fabricated with the highest level of



Fig. 10. Average hardness values of Fe-V₂AlC-GO composite.

Level	MT	CP	ST
1	16.64	16.41	16.40
2	16.39	16.70	16.54
3	16.49	16.42	16.58
Delta	0.25	0.29	0.17
Rank	2	1	3

Table 9. The response for density.

Level	MT	CP	ST
1	-18.90	-21.14	-21.23
2	-21.05	-18.28	-19.61
3	-20.60	-21.13	-19.71
Delta	2.14	2.86	1.61
Rank	2	1	3

Table 10. The response table for porosity.

compaction pressure had relative higher hardness. And previously stated that the highest density observed for S₇ but the highest hardness occurred for S₄, this indicated that distribution of particles was not uniform therefore analysis and optimization was needed to achieve optimal process parameters.

Analysis of density and porosity

The ANOVA was used to find the effect of parameters on multi-responses. The response table also provides the grades of influential parameters upon the responses as given in Tables 9 and 10.

The compaction pressure is the first influential parameter up on density and porosity, followed by milling time, and sintering temperature. It is obtained as A1B2C3 for experimental density. The Fig. 11, illustrated that the S/N ratio increased at the first level of MT, second level of CP and third level of ST.

Analysis of hardness

The influence of PM process parameters on the hardness clarified using the main effect plot for S/N ratios in Fig. 12, and larger the better criteria was used to analysis parameters. From the Table 11, the property of hardness mainly influenced by CP and followed by (ST and MT) respectively. And it reflected as the hardness property of the composites has a strong correlation with different process parameters.

The Fig. 12, below illustrated the correlation of process parameters and evaluated where the higher hardness achieved, on the figure milling time at first level, compaction pressure in the third and sintering temperature in the second level is the predicted correlation PM process parameters to increase hardness.

Therefore, the optimal parameter correlation generated through Taguchi analysis for hardness is A1B3C2. The ANOVA table for hardness tabulated below used to identify which controllable parameter significantly affects the performance characteristic.

Signal to noise (SN) ratio of the experiment values

In this study, density, porosity, and hardness responses were analyzed based on the GRA methodology. Fe-V₂AlC-GO composite with high density and hardness were desired, the higher-the-better criteria and lower-the-better criteria were applied for (density and hardness) and porosity respectively to convert the response data

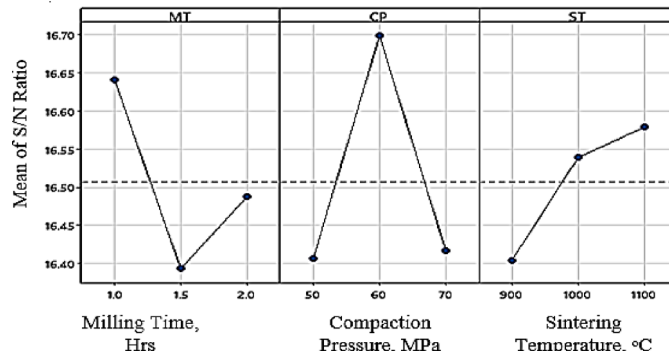


Fig. 11. Effect of process parameters on density (S/N ratio).

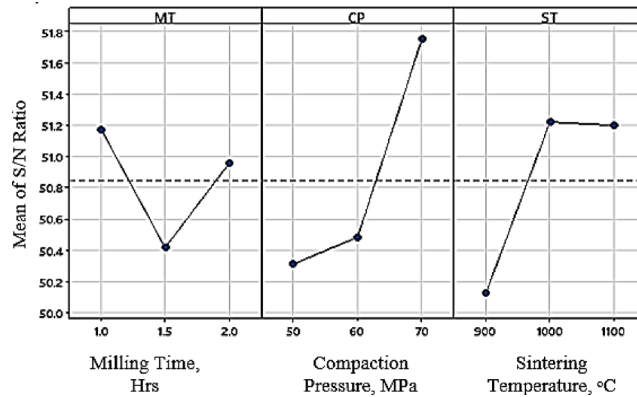


Fig. 12. Effect of process parameters on hardness (S/N ratio).

Level	MT	CP	ST
1	51.17	50.31	50.13
2	50.42	50.48	51.22
3	50.96	51.75	51.20
Delta	0.75	1.44	1.09
Rank	3	1	2

Table 11. The response table for hardness.

into the S/N ratio. The transformed density, porosity, and hardness response data into the S/N ratio are presented in Table 12. The S/N values of density and hardness were normalized as given in Table 13.

After the S/N ratio was normalized, the grey relation coefficient (δ_{ij}) was calculated to represent the relationship between the desired and actual experimental data. In situations where multiple factors need to be evaluated simultaneously, the grey relational coefficient allows for a comprehensive comparison of alternatives based on normalized data. This facilitates the identification of the best option among various choices. Finally, the grey relational grade (β_{ij}) was computed to summarize the overall performance of different experimental conditions. The grey relational grade enables the integration of various parameters' performance into a single value, thereby facilitating decision-making across various criteria. The calculated normalized S/N ratio, grey relational coefficient (δ_{ij}), and grey relational grade (β_{ij}) are shown in Table 14. The means of the grey relational grade for each level of controllable parameters were calculated and summarized in Table 14, the larger the grey relational grade shown in bold.

As shown in the response table for grade relation analysis compaction pressure is the first influential parameter, followed by sintering time and milling time respectively. To confirm optimal parameter of powder metallurgy process parameters ANOVA was needed for grey analysis grade was used to find out the contribution of process parameters. The results of ANOVA for the grey relational grade values are shown in Table 15. The results indicate that the percentage contribution of the MT, CP and ST are 11.42%, 65.63% and 19.81% respectively, the variation of compaction pressure is the highest influential parameter, followed by sintering time and milling time shown in Fig. 13, illustrated at what level the desired property of density, porosity and hardness to be achieved. Therefor

Sample	Experimental density	Porosity	Hardness
S ₁	16.54	-20.40	49.98
S ₂	16.09	-24.13	50.27
S ₃	16.37	-21.72	50.11
S ₄	16.44	-20.98	52.66
S ₅	16.76	-18.06	50.46
S ₆	16.52	-20.31	50.40
S ₇	16.93	-15.79	50.78
S ₈	16.12	-23.33	50.43
S ₉	16.53	-20.49	52.28

Table 12. S/N ratio of experimental responses.

Sample	Normalized S/N ratio (Y_{ij})			Grey relational coefficient (δ_{ij})			GRG (β_{ij})	Rank
	ρ	ϕ	HV	ρ	ϕ	HV		
S ₁	0.532	0.553	0	0.517	0.528	0.333	0.459	9
S ₂	0.000	1.000	0.111	0.333	1.000	0.360	0.564	4
S ₃	0.338	0.711	0.048	0.430	0.634	0.344	0.469	7
S ₄	0.420	0.622	1	0.463	0.570	1.000	0.677	1
S ₅	0.803	0.272	0.181	0.718	0.407	0.379	0.501	6
S ₆	0.516	0.542	0.158	0.508	0.522	0.373	0.468	8
S ₇	1.000	0.000	0.299	1.000	0.333	0.416	0.583	3
S ₈	0.032	0.904	0.167	0.341	0.838	0.375	0.518	5
S ₉	0.521	0.563	0.857	0.511	0.534	0.777	0.607	2

Table 13. Normalized S/N ratio, GRC and GRG.

Parameters	Level 1	Level 2	Level 3	Rank(max-min)
MT	0.573294	0.527965	0.514736	(3)0.058558
CP	0.48163	0.518003	0.616362	(1)0.134732
ST	0.497711	0.56949	0.548794	(2)0.071779

Table 14. Response table for grey relation analysis.

Source	DF	Seq SS	Adj MS	F-ratio	Contribution
MT	2	1.2562	0.6281	3.64	11.42%
CP	2	7.2183	3.6092	20.90	65.63%
ST	2	2.1789	1.0895	6.31	19.81%
Residual Error	2	0.3453	0.1727		
Total	8	10.9988			

Table 15. Results of the analysis of variance.

the optimal PM process parameters correlation identified from ANOVA analysis is A1B3C2 which is the same with previously identified optimal parameter through response table for grey relation analysis. As a result, the confirmation sample test were fabricated and evaluated with A1B3C2 (powder milled for 1 h, compacted at pressure of 70Mpa and sintered at temperature of 1000 °C with varying reinforcement 5%, 8%, 10%, 15% of V₂AlC and pure iron, fixed 4% of GO for all composition.

Physical and mechanical properties of samples at optimal level

The physical and mechanical properties of sintered samples were evaluated through previously discussed procedures in chapter three. The samples sintered with varying reinforcement (5%, 8%, 10%, and 15%) of V₂AlC with 4% GO as lubricant and pure iron were fabricated at optimal parameter (A1B3C2), denoted by S10, S11, S12, S13 and S14 respectively. From Table 16 and the Fig. 14a and b, below the density and porosity of samples were taken average value of three tested samples. The evaluated density values are (7.112, 7.019, 6.983, 6.691, and

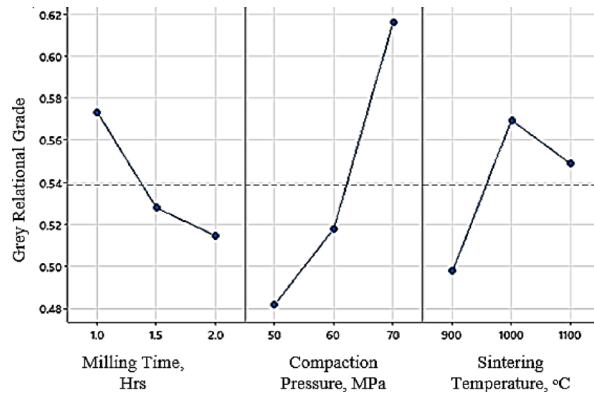


Fig. 13. Grey relational grade.

Sample	Density	Theoretical density	Porosity	Hardness (HV)
S ₁₀ (5% of V ₂ AlC)	7.112	7.4762	4.871459	423.8
S ₁₁ (8% of V ₂ AlC)	7.019	7.3856	4.963713	468.266
S ₁₂ (10% of V ₂ AlC)	6.983	7.3252	4.671545	534.2
S ₁₃ (15% of V ₂ AlC)	6.691	7.1742	6.735246	399.733
S ₁₄ (pure iron)	7.16	7.6272	6.125446	230.5

Table 16. Density, porosity and hardness value with varying reinforcement.

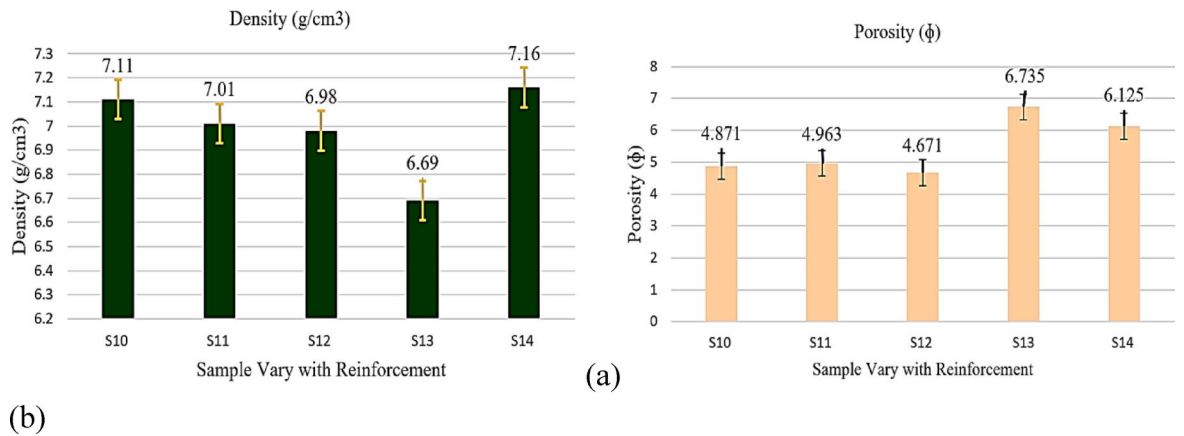


Fig. 14. (a) Density and (b) porosity value of varying reinforcement.

7.16) in g/cm³ for S10, S11, S12, S13 and S14 respectively. When the percentage of reinforcement increased the density of the samples decreases due the addition of low-density reinforcement compared with that of pure iron, in addition to that the percentage of porosity decreased up to 10% of reinforcement then it increases.

For sample S₁₃ porosity increased, this is due to increasing more percentage of reinforcement, as a result the volume fraction of the matrix decreases, this can lead to a reduction in the effective contact area between the base metal and the reinforcement particles, the particles are not well dispersed.

Hardness property of samples with varying reinforcement

Hardness is a very important characteristic in engineering applications as it indicates a material's ability to withstand friction, and erosion by external factors and iron-based material are applicable mainly for the application area which need more strength, to improve the hardness of material consequently improve the wear resistance, friction resistance, compressive strength and other related mechanical properties. Table 17. Shows the Vickers hardness of composite material with varying reinforcement.

From the Fig. 15a illustrated below the Vickers hardness of samples (S10, S11 and S12) increased when the reinforcement increases. The hardness of S10 is 423.8, the composition of the reinforcement was 5% V₂AlC, the same reinforcement with the first experiment. On the first experiment the highest hardness was studied on the

Sample	Trial 1	Trial 2	Trial 3	Average hardness
S10	418.8	424.7	427.9	423.8
S11	465.26	467.24	472.18	468.22
S12	531.8	534.7	536.2	534.2
S13	397.1	398.4	403.7	399.733
S14				230.5

Table 17. Vickers hardness of composite material with varying reinforcement.

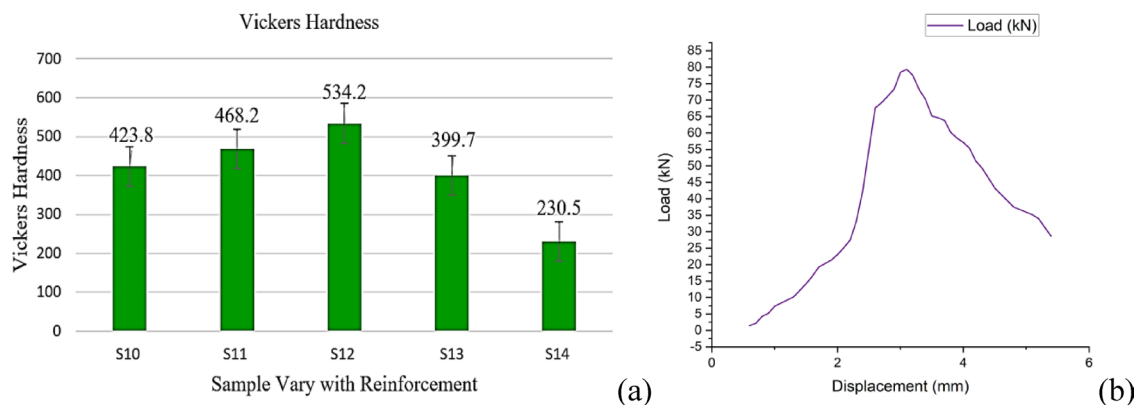


Fig. 15. (a) Hardness of composite material (b) Load displacement of Fe-10V2AlC-GO.

sample fabricated on S4 (A1B3C3) process parameters it was 429.833, this result with some extent greater than S10. S10 was fabricated on A1B3C2 optimal parameter and the desired density, porosity and hardness (7.112, 4.87 and 423.8). Generally improved optimal property occurred on S10 compared with S4. The highest hardness exhibited on S12 which is 10% of reinforcement then followed by S11 (8% reinforcement), the sintered sample of 15% V2AlC (S13) exhibited the reduced hardness but when compared with pure iron S13 exhibit improved hardness but it is smaller than S10. The graph of applied load versus displacement during this test is shown in Fig. 15b, The obtained maximum compressive strength was 702 MPa for S12 and followed by 585 MPa, 670 MPa, 570 MPa and 540 MPa for S10, S11, S13 and S14 respectively. The compression strength test was performed on the sample produced at optimum level using UTM following ASTM Standard B925-15. It has been observed that the addition of reinforcements Fe-10V2AlC-GO improves the ability of the iron to withstand compressive loads without failure. This indicated beyond 15% reinforcement of V2AlC the desired property will not be achieve, its hardness decrease, reduction on density due to voids (pores) and also increase porosity, with high reinforcement that leads to a reduction in an effective contact area between the matrix and reinforcement.

In this study of iron matrix composites reinforced with vanadium aluminum carbide and graphene oxide, it is observed that the properties of the Fe-10 V₂AlC-GO composite exhibit a density of 6.983 g/cm³, a porosity of 4.671%, a hardness of 534.2 HV, and a compressive strength of 702 MPa. However, when the reinforcement is increased to 15 wt.% (Sample S13), there is a noticeable decline in these properties, with the composite showing a density of 6.691 g/cm³, a porosity of 6.735%, a hardness of 399.733 HV, and a compressive strength reduced to 540 MPa. This data suggests that excessive reinforcement may adversely affect mechanical performance. The decline in mechanical properties at reinforcement levels exceeding 10 wt.% in iron-based composites can primarily be attributed to increased porosity, reduced matrix continuity, and agglomeration effects. This observation is consistent with findings in the literature^{9,10} which emphasize the necessity of optimizing reinforcement levels to achieve enhanced mechanical performance. For example, studies on MAX phase composites suggest that optimal reinforcement levels typically⁹ range between 5 and 15 wt.%. Beyond this threshold, properties such as hardness and tensile strength tend to decline due to similar factors including increased porosity and diminished matrix continuity. Furthermore, research on Fe-Al₂O₃ composites has reported significant reductions in hardness and strength when alumina reinforcement levels exceeded 10 wt.%, thereby corroborating the trends observed in our study¹⁰.

Corrosion resistance of composite material with varying reinforcement

A NaCl electrolyte were created by dissolving 3.5% of NaCl, and 150 mL of distilled water electrolyte was taken out for each experiment as given in Table 18. At a scan rate of 1 mV/sec, Potentio-dynamic polarization curves in the 250–250 mV region was captured for OCP. The Tafel Plot or polarization curve shown in Fig. 16a and b, (corrosion potential in Y-axis, versus corrosion current in X-axis). The Tafel estimation approach was applicable to detect Potentio-dynamic polarization in order to study the corrosion behavior of the manufactured samples. Calculating the rate of action of corrosion reactions can be done using the shape of the polarization curve.

Sample	E _{corr} (V)	I _{corr} (A/cm ²)	Corrosion rate (mpy)
S10	-0.694	657.819	1208.975
S11	-0.688	453.275	844.87
S12	-0.706	218.436	409.163
S13	-0.671	174.944	319.59
S14	-0.788	8050	14,705.87

Table 18. Corrosion rate.

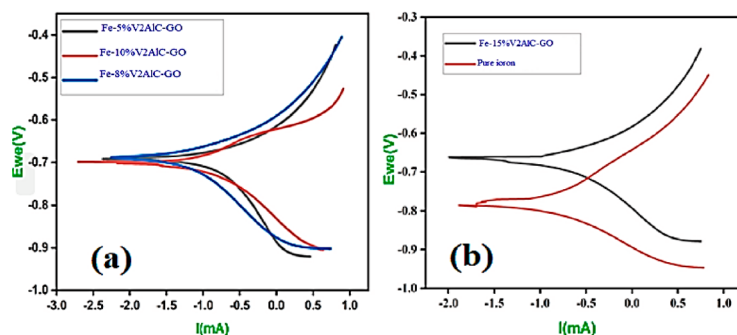


Fig. 16. (a) and (b) Corrosion potential E_{corr} for varying reinforcement.

From the Table 18, the calculated corrosion rate based on I_{corr} the small corrosion rate the higher performance to resist corrosion as a result S13 (Fe-15%V₂AlC-GO) exhibited the higher withstand corrosion and followed by S12 (Fe-10%V₂AlC-GO), S11 (Fe-8%V₂AlC-GO), S10 (Fe-5%V₂AlC-GO) and S14 (Pure iron). From the previous study on this paper S13 exhibited bad desired property therefore S12 is preferable.

Microstructural analysis

The sample, produced at an optimal level, underwent an optical microscope test to analyze the distribution of reinforcements within the base metal. The figure shows the OM micrograph of the composite material samples at different magnification levels. As the weight percentage of reinforcement, increase the porosity and more large grain are observed which may be due to the unreacted V₂AlC particle. From the Fig. 17, S12 well distribution reinforcement and no more porosity. On the other hand, S13 show more pores (voids) due to high percentage of reinforcement that leads to small contact to area between metal matrix and reinforcement.

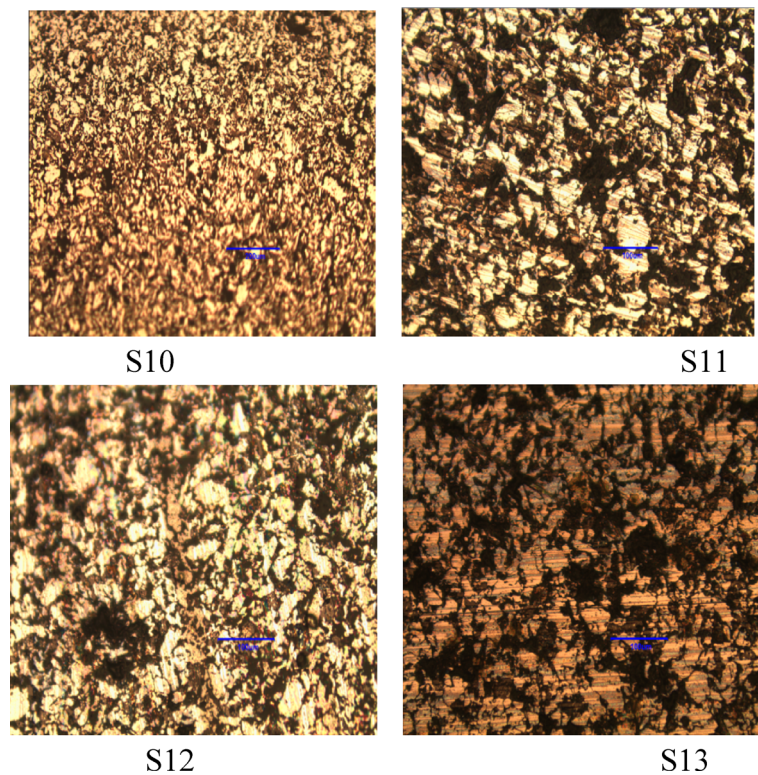


Fig. 17. OM image of composite materials.

X-ray diffraction (XRD) analysis

The X-ray diffraction (XRD) pattern of Fe-5V₂AlC-GO (S10), Fe-8V₂AlC-GO (S11), Fe-10V₂AlC-GO (S12) and Fe-15V₂AlC-GO were detected in angle between (10°-2θ-80°) at scan speed 3°/min. The samples' diffraction peaks were compared to XRD-JCPDS files of various materials, as shown Fig. 18. The XRD analysis show the existence of Fe (high intensity peak) and enhancements (V₂AlC and GO), which are symbolized by various signs and XRD-JCPDS, in the composite matrix.

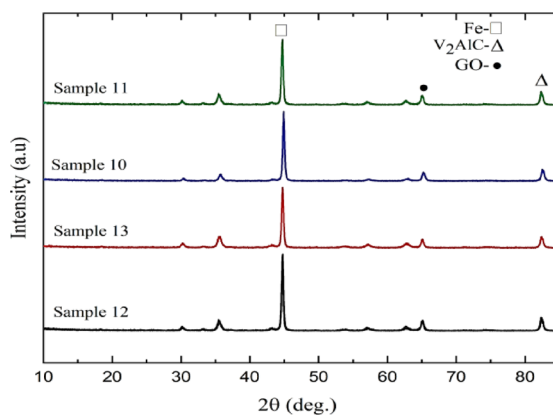


Fig. 18. XRD Spectrum of IMMC at different reinforcement content.

Crystalline sizes of sintered samples'

Crystalline size presented in Table 19, calculated for S12 (Fe-V₂AlC-GO), was used to determine crystalline size using the XRD data. Take K as 0.94 (recommended between (0.68–2.08) to calculate the Scherrer condition's

most extreme acceptable run for Fe- V₂AlC-GO (Lee et al., 2022), and since the average value is utilized, the diffraction peak point was calculated from the XRD data as 1.54056 (°), the X-ray diffraction wavelength, and as varied as possible. There is consistency between the average grain size and the average crystalline size value of 27.616 μm found in the XRD data.

Parameters		Data from XRD peak analysis			
K	λ (Å)	Peak position 2θ (°)	FWHM β (°)	D(μm) $D = \frac{K\lambda}{\beta \cos \theta}$	Average (D) (μm)
0.94	1.54056	44.8314	0.29	29.66	27.616
		44.9982	0.4602	24.7	
		46.4705	0.26	38.89	
		65.4829	0.3	29.06	
		65.6977	0.85	15.77	

Table 19. Crystalline size of Fe- 10V₂AlC-GO.

Conclusion

This study successfully fabricated iron metal matrix composites reinforced with V₂AlC and graphene oxide (GO) through a two-phase powder metallurgy approach. Initial experiments determined optimal process parameters—1 h milling time, 70 MPa compaction pressure, and 1000 °C sintering temperature—via Taguchi-based grey relational analysis, highlighting compaction pressure as the most influential factor for mechanical properties. Subsequently, varying V₂AlC reinforcement percentages revealed that the Fe-10 V₂AlC-GO composite (S12) exhibited superior physical and mechanical properties, including optimal density, porosity, hardness (534.2 HV), and compressive strength (702 MPa). Although Fe-15% V₂AlC-GO showed better corrosion resistance, its other properties were less desirable, making S12 the preferred material. Microstructural and XRD analyses confirmed homogeneous reinforcement distribution and the presence of V₂AlC and GO phases, substantiating the improved properties of the iron matrix. The research recommends a V₂AlC reinforcement range of 6–12%, with Fe-10 V₂AlC-GO identified as an excellent candidate for advanced applications, emphasizing the potential for further improvements through novel reinforcements and manufacturing techniques.

Data availability

The data will be made available on request from the Corresponding Author.

Received: 20 October 2025; Accepted: 23 December 2025

Published online: 10 January 2026

References

- Almadhoni, K. & Khan, S. Review of effective parameters of stir casting process on metallurgical properties of ceramics particulate Al composites. *IOSR J. Mech. Civil Eng.* **12**(6), 1684–2278 (2015).
- Aydogmus, T. Processing of interpenetrating Mg–TiNi composites by spark plasma sintering. *Mater. Sci. Eng., A* **624**, 261–270 (2015).
- Bhattacharyya, R., Iqbal, A., Gaur, T. & Gupta, P. Effect of ceramic reinforcement on the properties of iron based metal matrix nanocomposites. *Mater. Today: Proc.* **38**, 305–312 (2021).
- Chauhan, S., Verma, V., Prakash, U., Tewari, P. C. & Khanduja, D. Studies on induction hardening of powder-metallurgy-processed Fe–Cr/Mo alloys. *Int. J. Miner. Metall. Mater.* **24**, 918–925 (2017).
- Samal, P., Tarai, H., Meher, A., Surekha, B. & Vundavilli, P. R. Effect of SiC and WC reinforcements on microstructural and mechanical characteristics of copper alloy-based metal matrix composites using stir casting route. *Appl. Sci.* **13**(3), 1754 (2023).
- Das, A. K. Recent trends in laser cladding and alloying on magnesium alloys: A review. *Mater. Today: Proc.* **51**, 723–727 (2022).
- Das, B., Roy, S., Rai, R. N. & Saha, S. C. Development of an in-situ synthesized multi-component reinforced Al–4.5% Cu–TiC metal matrix composite by FAS technique—optimization of process parameters. *Eng. Sci. Technol. Int. J.* **19**(1), 279–291 (2016).
- Das, R., Mondal, M. K. & Pramanik, S. Strengthening behaviour and microstructural properties during the compaction of reduced blast furnace flue dust—fly ash—iron metal matrix composite fines using powder metallurgy route. *Trans. Indian Inst. Met.* **75**(9), 2255–2263 (2022).
- Gonzalez-Julian, J. Processing of MAX phases: From synthesis to applications. *J. Am. Ceram. Soc.* **104**(2), 659–690 (2021).
- Chaudhary, A. K., Gope, P. C., Mandal, A. K., Jain, V. & Patidar, A. Effect of feed rate and cutting speed on cutting forces developed during machining of epoxy based almond shell (*Prunus amygdalus L.*)—coconut fiber (*Cocos nucifera*) particle reinforced biocomposites. *Mater. Today: Proc.* **44**, 1903–1905 (2021).
- Edosa, O. O., Tekweme, F. K. & Gupta, K. A review on the influence of process parameters on powder metallurgy parts. *Eng. Appl. Sci. Res.* **49**(3), 433–443 (2022).
- Essien, U. A. & Vaudreuil, S. In-situ metal matrix composites development for additive manufacturing: a perspective. *J. Achiev. Mater. Manufact. Eng.* **111**(2), 78–85 (2022).
- Bhatti, J., Fazal, M. A., Bushroa, A. R., Khan, A. F. & Quazi, M. M. Structural and mechanical properties of (Cr, Ni) N single and gradient layer coatings deposited on mild steel by magnetron sputtering. *Tribology-Materials, Surfaces & Interfaces* **10** (3), 117–125 (2016).
- Gotaganaki, S., Mudakappanavar, V. S., Suresh, R. & Prasad, C. D. Studies on the mechanical properties and wear behavior of an AZ91D magnesium metal matrix composite utilizing the stir casting method. *Metallograp. Microstruct. Anal.* **12**(6), 986–998 (2023).
- Gupta, P., Kumar, D., Parkash, O. & Jha, A. K. Sintering and hardness behavior of Fe-Al₂O₃ metal matrix nanocomposites prepared by powder metallurgy. *J. Compos.* **2014**(1), 145973 (2014).
- Honnaiah, C., Srinath, M. S., & Lingappa, M. S. (2023). Metallographical characterization of Al-SiCP metal matrix composites processed through microwave sintering technique. *Materials Today: Proceedings*.

17. Hossein-Zadeh, M. et al. An investigation into the microstructure and mechanical properties of V2AlC MAX phase prepared by microwave sintering. *J. Alloy. Compd.* **795**, 291–303 (2019).
18. Hussain, M. Z., Khan, S. & Sarmah, P. Optimization of powder metallurgy processing parameters of Al₂O₃/Cu composite through Taguchi method with Grey relational analysis. *J. King Saud Univ. –Eng. Sci.* **32**(4), 274–286 (2020).
19. Khazaal, S. M., Nimer, N. S. M., Szabolcs, S. & Abdulsamad, H. J. Study of manufacturing and material properties of the hybrid composites with metal matrix as tool materials. *Results Eng.* **16**, 100647 (2022).
20. Kumar, A., Vichare, O., Debnath, K. & Paswan, M. Fabrication methods of metal matrix composites (MMCs). *Mater. Today: Proc.* **46**, 6840–6846 (2021).
21. Kumar, N., Bharti, A., Dixit, M. & Nigam, A. Effect of powder metallurgy process and its parameters on the mechanical and electrical properties of copper-based materials: Literature review. *Powder Metall. Met. Ceram.* **59**, 401–410 (2020).
22. Kumar, N., Bharti, A. & Saxena, K. K. A re-analysis of effect of various process parameters on the mechanical properties of Mg based MMCs fabricated by powder metallurgy technique. *Mater. Today: Proc.* **26**, 1953–1959 (2020).
23. Kumar, N., Bharti, A. & Saxena, K. K. A re-investigation: Effect of powder metallurgy parameters on the physical and mechanical properties of aluminium matrix composites. *Mater. Today: Proc.* **44**, 2188–2193 (2021).
24. Kumar, S., Singh, R. & Hashmi, M. S. J. Metal matrix composite: a methodological review. *Adv. Mater. Process. Technol.* **6**(1), 13–24 (2020).
25. Kumar, V. M. & Venkatesh, C. V. A comprehensive review on material selection, processing, characterization and applications of aluminium metal matrix composites. *Mater. Res. Express* **6**(7), 72001 (2019).
26. Lei, X. & Lin, N. Structure and synthesis of MAX phase materials: a brief review. *Crit. Rev. Solid State Mater. Sci.* **47**(5), 736–771 (2022).
27. Li, C. et al. Interfacial characteristics and wear performances of iron matrix composites reinforced with zirconia-toughened alumina ceramic particles. *Ceram. Int.* **48**(1), 1293–1305 (2022).
28. Li, Y. et al. Interfacial bonding and abrasive wear behavior of iron matrix composite reinforced by ceramic particles. *Materials* **12**(22), 3646 (2019).
29. Meignanamoorthy, M. & Ravichandran, M. Synthesis of metal matrix composites via powder metallurgy route: A review. *Mech. Mech. Eng.* **22**(1), 65–75. <https://doi.org/10.2478/mme-2018-0007> (2018).
30. Mohseni-Salehi, M. S., Taheri-Nassaj, E., Babaei, A. & Soleimanzade, M. Effect of different precursors on the formation and physical properties of V2AlC MAX phase. *J. Alloy. Compd.* **918**, 165588 (2022).
31. Mussatto, A., Ahad, I. U. I., Mousavian, R. T., Delaure, Y. & Brabazon, D. Advanced production routes for metal matrix composites. *Eng. Rep.* **3**(5), e12330 (2021).
32. Venugopal, M. M., Avilasha, B. G., Koti, V., Girisha, L., Rakesh, M., Shashidhara, L. C., ... & Udayashankar, S. (2024). Production and study of microstructure and mechanical characteristics of Al7075-boron carbide composites for automotive applications. *J. Inst. Eng. (India): Series D*, 1-10
33. Vijaya Kumar, R. et al. Experimental investigation of Al6063 alloy with zirconium silicate composite. *J. Inst. Eng. (India): Series D* **106**(2), 791–800 (2025).
34. Koti, V., Asha, P. B., Sharma, S., Kavitha, K., Sankarathil, A. J., Junaidi, M. A. R., & Udayashankar, S. (2025). Fabrication and wear characteristics of Al6066-boron carbide particulate composites. *J. Inst. Eng. (India): Series D*, 1-10.
35. Fayeka, M., Fazal, M.A. & Haseeb, A. S. M. A. Effect of aluminum addition on the electrochemical corrosion behavior of Sn–3Ag–0.5Cu solder alloy in 3.5 wt% NaCl solution. *Journal of Materials Science: Materials in Electronics* **27**(11), 12193–12200 (2016).
36. Kumar, D., Singh, S. & Angra, S. Dry sliding wear and microstructural behavior of stir-cast Al6061-based composite reinforced with cerium oxide and graphene nanoplatelets. *Wear* **516–517**, 204615 (2023).
37. Al Mahmood, A., Kader, M. A., Islam, M. B. & Hossain, R. Sustainable transformation of waste aluminium into high-performance composites: A review. *Int. J. Lightweight Mater. Manufact.* **8**(2), 194–204 (2025).
38. Kumar, Y. et al. Exploring MXenes and MAX phases: Advancements in properties, synthesis, and application. *Inorg. Chem. Commun.* **170**, 113531 (2024).
39. Sun, L. et al. Microstructure, phase composition, and current-carrying tribological performance of Ti–Al–TiC/C and Cu composite coatings. *Tribol. Int.* **214**, 111245 (2026).

Acknowledgements

Acknowledgments: a) The authors extend their appreciation to the Deanship of Research and Graduate Studies at King Khalid University for funding this work through Large Research Project under grant number RGP.2/291/46. b) This work was funded by the European Union under the REFRESH-Research Excellence for REgion Sustainability and High-tech Industries project number CZ.10.03.01/00/22_003/0000048 via the Operational Programme Just Transition. c) This work was supported by the National Research Foundation of Korea (NRF) grant funded by the Korea government (MSIT) (RS-2022-NR070832) and partly supported by YFL 2025, Yonsei University, Seoul, Korea,

Author contributions

Conceptualization: Engidayehu Mekonin Alemu (E.M.A) Jana Petrú (J.P) Muhammad Nasir Bashir (M.N.B) Abdulrahman Aljabri(A.A) Joon Sang Lee(J.S.L) Irfan Anjum Badruddin(I.A.B) Bilal Akbar Chuddher (B.A.C) M. A. Fazal (M.A.F) Sami Ghazali (S.G) Abdulmalik Alkotami (A.A.K) Gulam Mohammed Sayeed Ahmed (G.M.S.A.); Formal analysis Engidayehu Mekonin Alemu (E.M.A) Jana Petrú (J.P) Muhammad Nasir Bashir (M.N.B) Abdulrahman Aljabri(A.A) Joon Sang Lee(J.S.L) Irfan Anjum Badruddin(I.A.B) Bilal Akbar Chuddher (B.A.C) M. A. Fazal (M.A.F) Sami Ghazali (S.G) Abdulmalik Alkotami (A.A.K) Gulam Mohammed Sayeed Ahmed (G.M.S.A.); Resources: Engidayehu Mekonin Alemu (E.M.A) Jana Petrú (J.P) Muhammad Nasir Bashir (M.N.B) Abdulrahman Aljabri(A.A) Joon Sang Lee(J.S.L) Irfan Anjum Badruddin(I.A.B) Bilal Akbar Chuddher (B.A.C) M. A. Fazal (M.A.F) Sami Ghazali (S.G) Abdulmalik Alkotami (A.A.K) Gulam Mohammed Sayeed Ahmed (G.M.S.A.); Software Engidayehu Mekonin Alemu (E.M.A) Jana Petrú (J.P) Muhammad Nasir Bashir (M.N.B) Abdulrahman Aljabri(A.A) Joon Sang Lee(J.S.L) Irfan Anjum Badruddin(I.A.B) Bilal Akbar Chuddher (B.A.C) M. A. Fazal (M.A.F) Sami Ghazali (S.G) Abdulmalik Alkotami (A.A.K) Gulam Mohammed Sayeed Ahmed (G.M.S.A.); Writing—Engidayehu Mekonin Alemu (E.M.A) Jana Petrú (J.P) Muhammad Nasir Bashir (M.N.B) Abdulrahman Aljabri(A.A) Joon Sang Lee(J.S.L) Irfan Anjum Badruddin(I.A.B) Bilal Akbar Chuddher (B.A.C) M. A. Fazal (M.A.F) Sami Ghazali (S.G) Abdulmalik Alkotami (A.A.K) Gulam Mohammed Sayeed Ahmed (G.M.S.A.); Writing—review & editing: Engidayehu Mekonin Alemu (E.M.A) Jana Petrú (J.P) Muhammad Nasir Bashir (M.N.B) Abdulrahman Aljabri(A.A) Joon Sang Lee(J.S.L) Irfan Anjum Badruddin(I.A.B) Bilal Akbar Chuddher (B.A.C) M. A. Fazal (M.A.F) Sami Ghazali (S.G) Abdulmalik Alkotami (A.A.K) Gulam Mohammed Sayeed Ahmed (G.M.S.A.)

Mohammed Sayeed Ahmed (G.M.S.A.); Project Administration: Engidayehu Mekonin Alemu (E.M.A) Jana Petrú (J.P) Muhammad Nasir Bashir (M.N.B) Abdulrahman Aljabri(A.A) Joon Sang Lee(J.S.L) Irfan Anjum Badruddin(I.A.B) Bilal Akbar Chuddher (B.A.C) M. A. Fazal (M.A.F) Sami Ghazali (S.G) Abdulmalik Alkotami (A.A.K) Gulam Mohammed Sayeed Ahmed (G.M.S.A.); Engidayehu Mekonin Alemu (E.M.A) Jana Petrú (J.P) Muhammad Nasir Bashir (M.N.B) Abdulrahman Aljabri(A.A) Joon Sang Lee(J.S.L) Irfan Anjum Badruddin(I.A.B) Bilal Akbar Chuddher (B.A.C) M. A. Fazal (M.A.F) Sami Ghazali (S.G) Abdulmalik Alkotami (A.A.K) Gulam Mohammed Sayeed Ahmed (G.M.S.A.)

Funding

The authors gratefully acknowledge the funding and support received from various institutions. This work was supported by the Deanship of Research and Graduate Studies at King Khalid University through Large Research Project grant number RGP.2/291/46. . The authors extend their acknowledgement to the financial support of the European Union under the REFRESH-Research Excellence For REgion Sustainability and High-tech Industries project number CZ.10.03.01/00/22_003/0000048 via the Operational Programme Just Transition. Furthermore, support was received from the National Research Foundation of Korea (NRF) through a grant funded by the Korea government (MSIT) (RS-2022-NR070832), and partly by YFL 2025, Yonsei University, Seoul, Korea.

Declarations

Competing interests

The authors declare that they have no competing interests.

Additional information

Correspondence and requests for materials should be addressed to J.P. or G.M.S.A.

Reprints and permissions information is available at www.nature.com/reprints.

Publisher's note Springer Nature remains neutral with regard to jurisdictional claims in published maps and institutional affiliations.

Open Access This article is licensed under a Creative Commons Attribution-NonCommercial-NoDerivatives 4.0 International License, which permits any non-commercial use, sharing, distribution and reproduction in any medium or format, as long as you give appropriate credit to the original author(s) and the source, provide a link to the Creative Commons licence, and indicate if you modified the licensed material. You do not have permission under this licence to share adapted material derived from this article or parts of it. The images or other third party material in this article are included in the article's Creative Commons licence, unless indicated otherwise in a credit line to the material. If material is not included in the article's Creative Commons licence and your intended use is not permitted by statutory regulation or exceeds the permitted use, you will need to obtain permission directly from the copyright holder. To view a copy of this licence, visit <http://creativecommons.org/licenses/by-nc-nd/4.0/>.

© The Author(s) 2025